American Mineralogist, Volume 84, pages 620–628, 1999

Dissolution of well and poorly crystallized kaolinites: Al speciation and effects of surface characteristics

SUSAN H. SUTHEIMER,[1] PATRICIA A. MAURICE,[2,*] AND QUNHUI ZHOU[2]

[1] Department of Chemistry, Kent State University, Kent, Ohio 44242, U.S.A.
[2] Department of Geology, Kent State University, Kent, Ohio 44242, U.S.A.

ABSTRACT

This study compared surface characteristics and dissolution behavior of well-crystallized (KGa-1b) and poorly crystallized (KGa-2) kaolinite standards. Atomic force microscopy (AFM) revealed that particles of KGa-1b generally have nicely hexagonal micromorphology and crystallographically controlled microtopographic features. Particles of KGa-2 are also hexagonal, but their micromorphology tends to be more rounded. Basal-plane surfaces tend to be more irregular with fewer clearly crystallographically controlled features. KGa-1b particles tend to be larger in diameter and thicker than KGa-2 particles. Micromorphologic measurements showed that both KGa-1b and KGa-2 have modal edge- to total surface-area ratios of approximately 0.1 (mean ~ 0.2), although these measurements did not include the potentially large contribution of basal-plane step edges (additional 20% or more).

Dissolution experiments were conducted in oxalic acid and inorganic acids at pH 3, 22 °C, I = 0.01 *M*, under batch dissolution conditions. Dissolution rates (measured as Si release) in 1 m*M* oxalic acid were approximately twice as fast for KGa-2 as for KGa-1b (2.27 vs. 0.96 nmol/m^2·h). Rates for KGa-2 and KGa-1b were similar in HNO_3 (0.86 and 1.16 nmol/m^2·h, respectively). The comparable rates for these two sedimentary kaolinites and for a hydrothermal kaolinite studied by Wieland and Stumm (1992) suggests that the fundamental structure of kaolinite, rather than specific surface details, exerts the greatest influence on dissolution kinetics.

High-performance cation exchange chromatography (HP-CEC) was used to determine the distributions of monomeric Al species over the course of kaolinite dissolution. For dissolution in 1 m*M* oxalate, Al-oxalates were observed almost exclusively in agreement with results of equilibrium speciation calculations. For dissolution in HNO_3, the peak representing uncomplexed Al species, Al_f, was predominant but not exclusive, as predicted by calculations. A peak having a retention time characteristic of species with +2 charge may be evidence for an $AlOSi(OH)_3^{2+}$ species, and warrant further investigation.

INTRODUCTION

Kaolinite is one of the most abundant aluminosilicate minerals, occurring primarily as clay-sized particles with high surface-area-to-volume ratios. Hence, kaolinite weathering may play an important role in controlling the chemical characteristics of natural waters and the evolution of soils. Natural kaolinites exhibit a range of characteristics, such as degree of crystallinity, points of zero charge, concentrations of impurities, particle size distributions, and particle aspect ratios (e.g., Schroth and Sposito 1997; Zhou 1996). Although kaolinite dissolution kinetics in inorganic acids (proton promoted dissolution) and organic acids (ligand promoted dissolution) were studied previously (e.g., Carroll-Webb and Walther 1988; Chin and Mills 1991; Nagy et al. 1991; Wieland and Stumm 1992; Ganor et al. 1995; Schroth and Sposito 1997), we do not yet understand how natural kaolinite variability may contribute to differences in field and laboratory dissolution rates. Because the dissolution of kaolinite appears to be surface-reaction controlled (Carroll-Webb and Walther 1988; Wieland and Stumm 1992; Xie and Walther 1992; Ganor et al. 1995), differences in surface properties can be expected to influence dissolution rates (e.g., Hochella 1990).

The first objective of the present study was to determine how variations in surface characteristics and crystallinity of two Georgia kaolinites influenced kaolinite dissolution (measured by Si release) in batch experiments with inorganic and organic (oxalate) solutions at pH = 3 and 22 °C. Prior to dissolution experiments, atomic force microscopy (AFM) was used to characterize the morphology and microtopography of well crystallized (KGa-1b) and poorly crystallized (KGa-2) standard kaolinites. BET analysis was used to determine the specific surface areas, and X-ray diffraction (XRD) to determine the degree of crystallinity. The second objective was to apply newly developed high-performance cation exchange chroma-

[1] Present address: Notre Dame College of Ohio, South Euclid, Ohio 44121-4293, U.S.A.
*E-mail: pmaurice@kent.edu

tography (HP-CEC) methods to determine the distribution of monomeric aluminum species formed over the course of kaolinite dissolution. This technique permitted monomeric Al determinations at levels as low as 7 n*M* (Sutheimer and Cabaniss 1995b) and provided new insight into dissolution processes.

MATERIALS AND METHODS

Kaolinite standards

Two standard kaolinite samples from The Clay Minerals Society were used. KGa-1b is a well crystallized kaolinite from Washington County, Georgia. KGa-2 is a poorly crystallized kaolinite from Warren County, Georgia. Descriptions as "well" vs. "poorly" crystallized are discussed by Van Olphen and Fripiat (1979). The kaolinite samples were characterized prior to the reaction, using a variety of techniques. Details of sample characterization are provided in Zhou (1996); brief descriptions are provided below.

X-ray diffraction analysis (XRD) performed on a Rigaku X-ray diffractometer (Geigerflex, Inc.) in the Department of Geology, Kent State University, showed that KGa-1b contained a small amount of halloysite, whereas KGa-2 contained traces of anatase.

Clay samples were cleaned prior to dissolution experiments to remove amorphous oxyhydroxide material, as follows. Kaolinite (100 g) was added to 1 L of 1 *M* NaCl solution that had been adjusted to pH 3.0 with HCl. The suspension was stirred using a floating magnetic stirring bar for approximately one hour, allowed to settle overnight, and the supernatant removed by vacuum suction. This procedure was repeated four times until the pH of the supernatant was 3.0. The clay was then washed repeatedly in Milli-Q UV (UV referring to ultraviolet treatment to remove organics) water until the conductivity of the supernatant decreased to 300 μS/cm for KGa-1b and 695 μS/cm for KGa-2, and the pH was higher than 5.5. Separated solid kaolinite was air dried. The average diameters and thickness of the two cleaned kaolinites as measured by AFM were found to be less than those of the initial samples (Table 1); the cleaning procedure apparently caused particles to become more dispersed.

Determination of the points of zero charge of kaolinite was problematic. For example, Schroth and Sposito (1997) showed that the point of zero net proton condition (p.z.n.p.c.) for kaolinite varied with equilibration time. We determined values of p.z.n.p.c. by titration. Prior to titration, our samples were allowed to "equilibrate" with a N_2-purged, near neutral solution overnight, and then pH was dropped to 3 and samples were repurged prior to and during titration. Total titration time for each sample was approximately 3 h. Further specifics of titrations and calculations are provided by Zhou (1996). We determined values of p.z.n.p.c. for cleaned KGa-1b and KGa-2 of 5.1 ± 0.2 and 4.9 ± 0.2 respectively. These values are in reasonably close agreement with Schroth and Sposito's (1997) "equilibrium" p.z.n.p.c. values of 4.99 ± 0.03 and 5.36 ± 0.2 for KGa-1 (a similar sample to KGa-1b) and KGa-2 respectively. However, more detailed analysis of our samples in the manner of Schroth and Sposito (1997) would be required to compare results directly.

Batch dissolution procedure

Although several researchers have pointed out the shortcomings of batch dissolution experiments (e.g., Chou and Wollast 1985; Rimstidt and Dove 1986; Brantley and Chen 1995; Ganor et al. 1995) we chose to use batch reactors because of their simplicity and because our experiments dealt with initial dissolution conditions, at low pH and far from equilibrium, where accumulation of reaction products should be minimized. Dissolution vessels consisted of Fisher brand high-density polyethylene (HDPE) 1 L wide-mouth bottles, which were no more than half filled with solution. Samples were stirred using floating PTFE-coated magnetic stirrers. Temperature was controlled by pumping water from a constant-temperature water bath through coils of Nalgene tubing, which encircled the covered reaction bottles. All containers were washed with phosphate-free detergent, rinsed repeatedly with deionized water, acid-washed in 10% nitric acid, rinsed repeatedly with Milli-Q UV water, and air dried under protective cover before use.

Dissolution experiments were carried out at 22 ± 0.05 °C, pH 3.0, with ionic strength (*I*) adjusted to 0.01 *M* using $NaNO_3$ (or NaCl, for the HCl experiment). All experiments contained

TABLE 1. Properties of kaolinites used in dissolution experiments

Property	KGa-1b	KGa-2	KGa-1b cleaned	KGa-2 cleaned
Number of samples	170	170	92	127
diameter range (nm)	109-3586	78-1811		
mean diameter (nm)	785 (39)	447 (27)	586 (42)	359 (29)
modal diameter (nm)	420	200		
thickness range (nm)	11-143	10-174		
mean thickness (nm)	58 (2)	42 (2)	41 (2)	37 (3)
modal thickness (nm)	37	22		
edge steps	linear	curved	linear	curved
micromorphology	hexagonal	rounded hexagonal	hexagonal	rounded hexagonal
microtopography	crystallogr. control	rounded	crystallogr. control	rounded
mean ratio-edge to total surface area†	0.17 (0.01)	0.18 (0.01)	0.17 (0.01)	0.19 (0.01)
modal ratio-edge to total surface area†	0.10	0.12	0.14	0.14
BET surface area (m^2/g)‡	12.5	22.4	12.6	22.2
p.z.n.p.c			5.1 ± 0.2	4.9 ± 0.2

Notes: All properties except for BET surface area, p.z.n.p.c., and structure measured by AFM*. Values in parentheses are standard errors.
*AFM measurements of diameter, thickness, and surface area ratios must be considered to be semi-quantitative, because of rigorous point-counting procedures were not possible due to particle aggregation and limitations imposed by the finite dimensions of AFM tips.
† These ratios are based on particle micromorphology and do not include contribution of basal plane edge steps.
‡ Zero net proton condition. Data from Bereznitski et al. (1998) on the same samples used in our study.Table 2. Kaolinite batch dissolution experiments: conditions and results.

3.0 g/L kaolinite in 300 mL of solution. Three sets of experiments (Table 2) were conducted that compared dissolution in an organic acid (oxalic) vs. an inorganic acid (HCl or HNO_3). The pH values of the reacting suspensions were adjusted using HNO_3 in all experiments except 1b, which used HCl. After this initial pH adjustment, the pH was maintained for two hours using an automated potentiostat, then allowed to drift (total pH drift over the course of experiments was 0.1 pH unit or less). Sample aliquots (15 to 20 mL) were removed periodically from the continuously stirred solutions for analysis. Aliquots were filtered sequentially through 0.4 μm and 0.1 μm Nuclepore polycarbonate (pc) membrane filters, which had been rinsed previously with Milli-Q UV water and air dried. Sample pH was measured immediately on filtered samples. Aliquots were then stored at 4 °C and analyzed for Al and Si within 72 hours.

All reagents were reagent grade or better unless otherwise noted. Al and Si standards were prepared from Fisher Scientific Atomic Absorption Standards (1000 mg/L). Sodium nitrate, nitric acid, and sodium oxalate were 99.999% pure from Aldrich Chemical (Milwaukee, Wisconsin). Lumogallion was obtained from TCI (Tokyo Kasei Kogyo Company, Ltd., Portland, Oregon). Reagents for silica determinations were obtained from Hach Company (Loveland, Colorado). All experiments used Milli-Q UV water.

Aluminum, silica, and oxalate determinations

The concentrations of monomeric Al fractions were determined using High-Performance Cation Exchange Chromatography according to the method of Sutheimer and Cabaniss (1995b). This method determines low (down to 7 n*M*) concentrations of either complexed or free Al^{3+} using a cation exchange chromatographic column, gradient elution ($CaCl_2$), and aluminum-specific post column detection with the fluorescent reagent lumogallion. Polymeric aluminum oxyhydroxide species are not detected by the HP-CEC method. Species elute from the column sequentially, generally as a function of size and charge (or polarity). Thus, the first peaks eluting from the column have a charge of +1 or less. Intermediate peaks have a charge of +2. Finally, uncomplexed Al^{3+} and its monomeric hydrolysis species (collectively referred to as Al_f) elute at ~12 min. The RSD (relative standard deviation) of a 3.7 μ*M* Al standard analyzed nine times over two days was 3.5%. Al standards (0.37, 3.71, and 37.1 μ*M*) for determining concentrations of Al fractions were prepared immediately prior to use from AA Standard Solution (1000 mg/L) in pH 3.0 HNO_3 and 1 m*M* oxalic acid, in PTFE beakers. Standard curves (peak area vs. concentration) routinely had r^2 values = 0.999 as determined by least squares linear regression, although the standard concentrations were not distributed normally. Total monomeric Al was calculated as the sum of concentrations of all forms of Al determined by HP-CEC.

To determine the effects of sample filtration on the concentration of Al in solution, standards were prepared in pH 3.0 HNO_3 with and without 1 m*M* oxalate. Total areas (the summation of areas of chromatographic peaks) were less when filtered. Differences were about 15% for the 0.37 μ*M* standard and about 3% for the 37.1 μ*M* standard, indicating some absorption by the polycarbonate membrane during filtration. Nevertheless, we judged that filtration was a better means of separation than centrifugation because it is presently unknown whether centrifugation might alter distributions of Al monomeric/polymeric species.

Silica was determined using the "Heteropoly Blue" method according to the Hach Company "Silica DR/3000" Procedure, (low range, 0 to 2000 μg/L) Code S.3 but using 1 cm quartz sample cells and an Hitachi U-2000 spectrophotometer to determine absorbance. Silica standards were prepared from Fisher Silica Atomic Absorption Standard (1000 mg/L) in pH 3.0 HNO_3. The RSD for this analysis was shown to be 5.5% for the 100 μg/L standard. Concentrations of filtered and unfiltered standards were nearly identical.

Oxalate concentrations of filtered aliquots were determined using a Shimadzu TOC5000 carbon analyzer. This technique provided total dissolved organic carbon concentrations and was not specific to oxalate.

Atomic force microscopy

AFM was performed using a Digital Instruments (DI) Nanoscope III AFM with an optical microscope attachment and TappingMode (Digital Instruments, Inc.) capability. A description of the system and its application to environmental particles can be found in Maurice (1996). Both contact mode and TappingMode (TMAFM) were used, and all imaging was performed in air. TMAFM allows high-resolution topographic imaging of soft, adhesive, or fragile samples, because it overcomes problems associated with friction, adhesion, and electrostatic forces (Prater et al. 1995). For contact mode, DI silicon-nitride (Si_3N_4) tips were used; for TMAFM, silicon (Si) tips were used. Tip dimensions are described in detail in Maurice and Lower (1997) and at Digital Instrument, Inc.'s worldwide web site (http//www.di.com).

TABLE 2. Kaolinite batch dissolution experiments: conditions and results

Expt.	Sample	Ligand or acid	Ligand conc. *(M)*	Dissolution period (h)	Al rate (nmol/m^{2s}·h)	Si rate (nmol/m^2·h)
1a	KGa-1b	Oxalate	0.005	486	2.27 ± 0.17	
1b	KGa-1b	HCl	0.001	486		
2a	KGa-1b	Oxalate	0.001	328	1.31 ± 0.10	0.96 ± 0.05
2b	KGa-1b	HNO_3	0.001	328		1.16 ± 0.07
3a	KGa-2	Oxalate	0.001	312	2.66 ± 0.20	2.27 ± 0.13
3b	KGa-2	HNO_3	0.001	312		0.86 ± 0.05

Notes: All solutions contained 3.0 g/L kaolinite and were conducted at pH 3, I 0.01 *M*, and 22 °C. $NaNO_3$ was used as the background electrolyte. Rates calculated based on data collected at 24 hours and longer expect as indicated below.

TMAFM imaging of particles was generally conducted simultaneously in the so-called height and amplitude modes. The amplitude mode gives essentially the first derivative of the topographic data and hence tended to highlight edges and fine structures. However, in amplitude mode images, the height (*z*-range) data were inaccurate and hence *z* scales are not shown herein.

Samples were prepared for AFM analysis by dispersing a very small amount (<10 mg) of kaolinite in 20 mL of Na_2PO_3 solution made with Milli-Q UV water. The samples were ultrasonicated for 2 min. One or two drops of kaolinite suspension were then placed on previously cleaned glass slides or on freshly cleaved muscovite and allowed to air dry under protective cover. Additionally, some samples were filtered from suspension onto 0.1 μm Nuclepore polycarbonate membrane filters, air was forced through the filters to dry, and the membranes were allowed to complete drying under protective cover prior to analysis. Particle dimensions were measured only on the glass- or muscovite-mounted specimens, as the membranes were too irregular to allow for detailed measurements.

Speciation analysis

Estimates of species distributions were made using the computer program TITRATOR (Cabaniss 1987) with aluminum hydrolysis constants listed in Sutheimer and Cabaniss (1995b). Other necessary constants are listed in Table 3. The calculations neglect the effects of surface reaction and species and assume that Al-nitrate, Al-silicate, and Si-oxalate species are weak or lacking.

TABLE 3. Additional formation constants used for equilibrium calculations

Reaction	log K	Reference
$HOx^- + H^+ \leftrightarrow H_2Ox$	1.2	Drever (1988)
$Ox^{2-} + H^+ \leftrightarrow HOx^-$	4.2	Drever (1988)
$Al^{3+} + O^{2-} \leftrightarrow AlOx^+$	5.97	Martell et al. (1993)
$Al^{3+} + 2O^{2-} \leftrightarrow AlOx_2^-$	10.93	Martell et al. (1993)
$Al^{3+} + 3Ox^{2-} \leftrightarrow AlOx$	15.97	Martell et al. (1993)

RESULTS AND DISCUSSION

Characteristics of kaolinite samples

The two kaolinites display different crystallinity, particle sizes, microtopography, micromorphology, and specific surface areas as determined by XRD, AFM, and/or BET measurements (Table 1). In general, the KGa-1b particles are larger in diameter and thicker than the KGa-2 particles, resulting in larger specific surface and edge areas for the latter (Table 1). AFM measurements of diameter, thickness, and surface area ratios must be considered to be semi-quantitative, because rigorous point-counting procedures were not possible due to particle aggregation and limitations imposed by the finite dimensions of AFM tips. More thorough AFM measurements and analysis are currently underway.

TMAFM amplitude-mode images of well-crystallized kaolinite, Kga-1b (Figs. 1a, and 1b) showed particles with generally nicely hexagonal micromorphology and crystallographically controlled microtopographic features. Crystal angles between two ajacent edge surfaces [(011) and (010)] on the (001) basal planes are measured as 111° to 129°, often ~ 120° (120° being an hexagonal angle). In some instances (Fig. 1b), it was difficult to determine whether hexagonal features on particle surfaces are microtopographic features or smaller, adhering kaolinite particles. This problem could lead to biases in grain-size measurements. Booksheets packeting of particles often was observed (not shown here).

Many basal-plane surfaces contain straight-edged steps showing clear crystallographic control (Figs. 1a, and 1b); such features most probably are relict growth structures. Most steps were approximately 1 to 3 unit cells thick. In general agreement with our work, Zbik and Smart (1998) reported unit-cell-high steps on North Queensland kaolinite. It is possible that atomic-scale steps are present on KGa-1b, but we have found in our own experience and in the literature (e.g., Zbik and Smart 1998) that most height-mode AFM images are of insufficient quality to support height measurements at the atomic scale. Some hexagonally shaped features that are much thicker (tens of unit cells) may be small adhering kaolinite particles rather than actual steps. We observed both pancake-like steps indicative of a birth-and-spread growth mechanism and spiral growth structures. Blum (1994) observed some spiral steps on illite, and he reported that the spiral step edges had a distinctive, sawtooth roughness. Such roughness has been attributed to adsorption of impurities during growth processes, which may poison growth along a step (e.g., Berner and Morse 1974; Dove and Hochella 1993; Blum 1994). In contrast to Blum's observations, step edges on KGa-1b tended to be smooth with only an occasional kink. This suggests that potential poisoning impurities were more-or-less absent during the growth process.

Poorly crystallized kaolinite particles (KGa-2) (Figs. 1c, 1d, and 1e) tend to be smaller and thinner than particles of KGa-1b. Whereas the overall grain shape of KGa-2 is also hexagonal, most particles have more irregular or rounded outlines. Edge steps tend to be curved, and surfaces have a more irregular appearance than observed on KGa-1b. Basal-plane surface microtopography tends to be rounded with little or no clear, crystallographically controlled features. Many rounded features are present with topography on the scale of a few nanometers. In some cases (e.g., Fig. 1e), pancake-type islands appear on basal-plane surfaces. However, in a case such as shown in Figure 1e where the outline doe not match the underlying particle outline, it is difficult to be certain whether islands are microtopographic growth features or adhering particles. In many cases, small particles can clearly be discerned, attached to the basal-plane surfaces of larger particles. These small particles are on the order of 20 nm thick. Aggregates consist of variously sized crystals (Fig. 1d); booksheets packeting was not observed.

Based on micromorphologic measurements, we estimated modal and mean edge-to-total surface-area ratios. These ratios (Table 1) do not include the potentially substantial contribution of basal-plane step edges. For KGa-1b, we estimate approximately 20% additional edge surface area from basal-plane step edges. Microtopography of KGa-2 particles is so irregular that it is difficult to estimate the contribution of basal-plane step edges; we roughly estimate 20 to 30% additional edge surface area from basal-plane step edges. Our results (Table 1) are in agreement with AFM results on KGa-1 by Brady et al. (1996) who reported percentage edge areas of 10 to 50% but

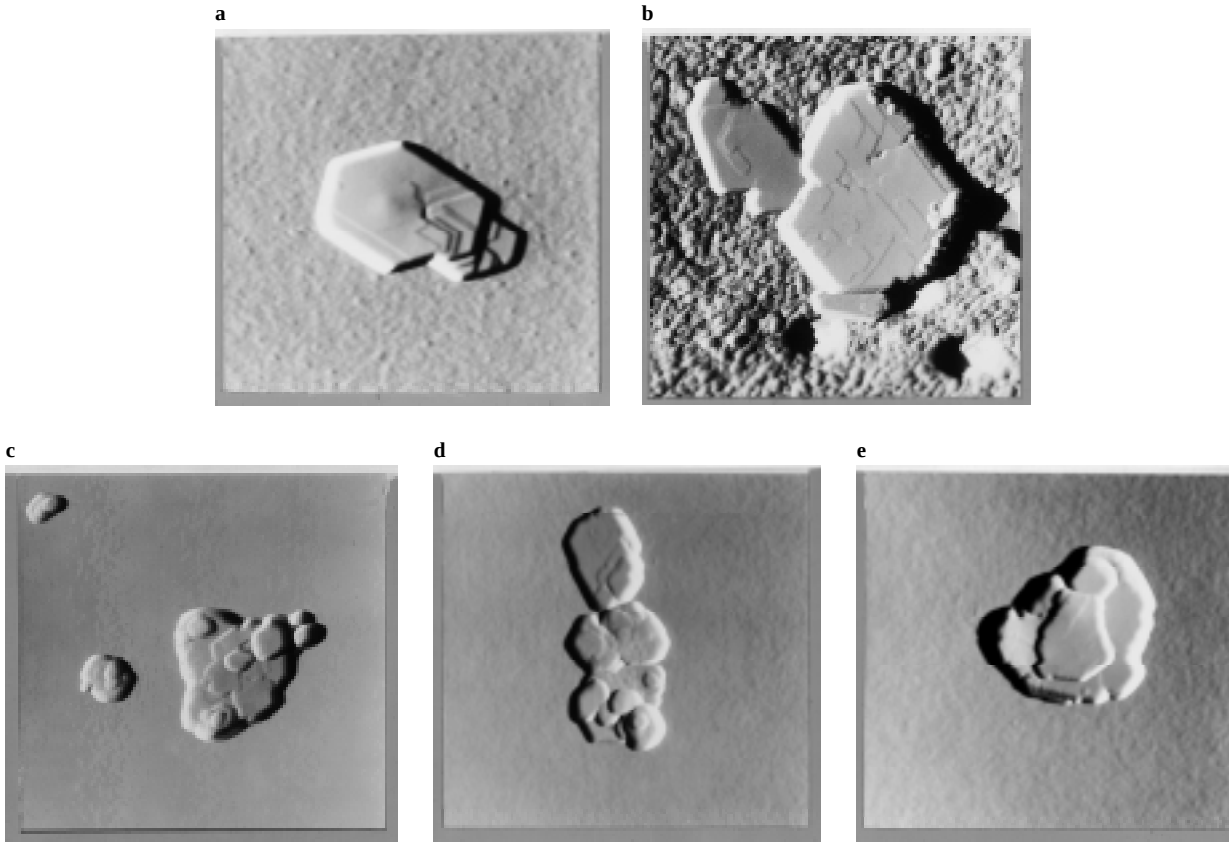

FIGURE 1. Amplitude mode TMAFM images of kaolinite samples used in these experiments. **(a** and **b)** KGa-1b; **(c, d,** and **e)** KGa-2. Image dimensions are **(a)** 900 nm, **(b)** 1.25 μm, **(c)** 2.5 μm, **(d)** 1.3 μm, **(e)** 1.0 μm, on a side. Height data are not provided because the amplitude mode distorts height data. Sample shown in b was mounted on a polycarbonate membrane (note pores); other samples were mounted on glass slides. Measurements made on height mode data reveal that the large particle shown in **a** is ~50 nm thick; steps on the surface of this particle are ~1.4 nm high (2 unit cells). The large particle on the right-hand side of **b** is ~70 nm thick; the smaller particle to the left is ~20 nm thick. Steps are ~1 to 2 nm high (1 to 3 unit cells). The large particle in **c** is 100 to 120 nm thick, and the smaller (probable) particles adhering to the surface are 20 to 30 nm thick. The smaller particle just left of center is 70 nm thick, with smaller 20 nm thick particles adhering to the surface. The larger particles in **d** are ~50 nm thick, whereas the smaller particles are ~20 nm thick. The particle in **e** is ~45 nm thick along the edge, and the pancake like feature on the surface (an island or an adhering particle) is ~10 nm thick. Depending upon scan direction (left-right or right-left), particle images contained artifacts consisting of a light edge and a shadow on either side (left or right). The light edges also tended to be sloping due to tip-sample shape interaction, which distorts the actual particle shape. See Maurice (1996) for detailed descriptions of AFM artifacts on particle images.

small sample sizes. Our estimates broadly agree with Zbik and Smart's (1998) estimate of total edge site contribution above 30% of total surface area for a poorly crystallized North Queensland kaolinite. Results from all three groups suggest that edge sites represent a larger contribution to kaolinite's total site density than previously thought. Surface microtopographic features were similar for original (uncleaned) and cleaned samples, suggesting that the observed microtopographic features described above were not induced by the cleaning procedure.

Monomeric aluminum speciation over the course of dissolution

Chromatograms of Al species determined during dissolution experiments show that for kaolinite in oxalic acid, the predominant species is represented by the peak at the void volume of the system, 3.2 min (Fig. 2a). This peak represented the combined concentrations of Al-Ox^{+}, Al-Ox_2^{1-}, and $AlOx_3^{3-}$ (where Ox^{2-} is the dideprotonated oxalate). For a detailed discussion of HP-CEC peak assignments, see Sutheimer and Cabaniss (1995a,1995b). Speciation calculations indicated that these Al-oxalate species should constitute >99% of the total Al for total Al concentrations of 1 to 100 μ*M* under our experimental conditions. Because the aqueous Al-oxalate species predominated (Fig. 2), it is clear that they reached equilibrium quickly, being controlled by thermodynamic processes. The observation of Al-oxalates in solution is consistent with the mechanism proposed by Wieland and Stumm (1992), wherein oxalate forms surface complexes with Al sites on the kaolinite surface and then detaches as a complex into solution. However, because Al-oxalate equilibration in solution is fast, we could not determine whether the Al-oxalate complexes formed as part of the dissolution process or subsequently from Al and oxalate in solution.

In contrast, the major species found experimentally for proton-promoted kaolinite dissolution (in inorganic acids) include uncomplexed Al or Al_t, species virtually absent in the oxalate

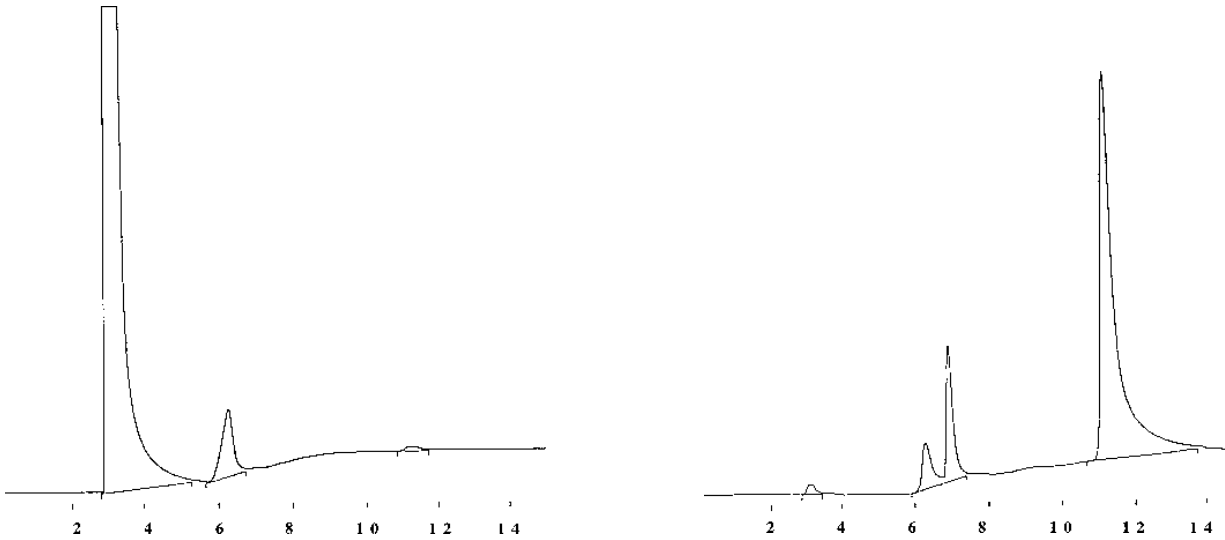

FIGURE 2. (a) HP-CEC chromatogram of KGa-1b dissolved in 5 m*M* oxalic acid at pH 3, I = 0.01. **(b)** HP-CEC chromatogram of KGa-1b dissolved in pH = 3, I = 0.01 HNO_3. See text for a detailed explanation of the peaks.

dissolution solutions (Figs. 2 and 3). Al_f, uncomplexed Al^{3+}, and its pH dependent hydrolysis species $Al(OH)^{2+}$, $Al(OH)_2^+$, $Al(OH)_3$, and $Al(OH)_4^-$ is represented by the peak at 11.8 min. These results were consistent with the absence of the strongly complexing oxalate ligand, which was the controlling factor in the distribution of Al species under the oxalate experimental conditions.

A small peak (~0.7 μ*M*) with a retention time of approximately 6.2 min may result from $AlCl^{2+}$ (a result of the washing procedure) and/or AlF^{2+} from trace F^- occurring in KGa-1b. The small concentrations of Al represented by this peak are probably not important for understanding the dissolution process.

Another small peak occurred at a retention time of ~7.0 min and also represented an Al species with a charge of +2 (Fig. 2b). This peak was virtually absent in the presence of oxalate (Figs. 2a and 3b) except for initially low concentrations for KGa-1b dissolved in 1 m*M* oxalate. In contrast, small amounts (generally <1 μ*M*) occurred when oxalate was not present. This species appears at the retention time assigned by Sutheimer and Cabaniss (1997) to $AlOSi(OH)_3^{2+}$. Although evidence that this species is present in our reacting solution is compelling, it is not definitive. Because the formation constant,

$$K_f = \frac{[AlOSi(OH)_3^{2+}][H^+]}{[Al^{2+}][Si(OH)_4]}$$

for this species is small ($\log K_f < -1$), one would not expect it to form from Al^{3+} and $Si(OH)_4$ in solution. Rather, this species might conceivably form as part of the dissolution process as a metastable reaction product. If this is true, then its dissociation to Al^{3+} and $Si(OH)_4$ components must be slow enough to maintain a detectable concentration in our experiments.

Although the HP-CEC technique does not measure polymeric Al, we anticipated negligible concentrations. Based on the formation constant for the $Al_2(OH)_2^{4+}$ dimer, as reported by Sutheimer and Cabaniss (1997), and the pH and Al^{3+} concentrations measured herein, we calculate equilibrium dimer concentrations at least two orders of magnitude lower than Al^{3+} concentrations throughout our experiments.

Si concentrations

Si concentrations increase with time (Fig. 3d). By the end of the experiments (after 320 hours of dissolution), Si concentrations were similar for KGa-1b in 1 mM oxalate, KGa-1b in HNO_3 and KGa-2 in HNO_3. Si concentrations were approximately four times higher for KGa-2 in 1 m*M* oxalate.

Dissolution rates in organic and inorganic acids

Concentrations of total (monomeric) Al and total Si released as a function of time, normalized to BET specific surface areas, are shown in Figure 4. Dissolution rates are designated R_{mAl} when monitored using Al concentrations and R_{Si} when monitored using Si concentrations. (The mAl subscript refers to the fact that the rate is based on monomeric Al and does not include any polymeric forms, although we do not anticipate polymeric Al based on equilibrium calculations.) Dissolution rates were initially high in all cases except for Al in inorganic acid (for which no rate was calculated) and for all but the Al inorganic case, reached an apparent steady state after 24 h of dissolution. For Al in inorganic acid, we could not determine whether steady state was achieved based on our experimental data. After apparent steady state was achieved (~24 h) in the other data sets, the dissolution reactions (Figs. 4a, 4b, and 4d) may be interpreted in terms of zero-order kinetics with respect to the total number of surface sites, assuming that the mole fraction of active sites and the specific surface area remain constant after this time. The release rates (Table 2) are compared in greater detail below. We calculate that the bulk solutions remained well below saturation with respect to kaolinite throughout our experiments. Our dissolution rates in oxalate at pH 3 are within a factor of 2 lower than Wieland and Stumm's (1992) reported rates for dissolution of Cornwall kaolinite. The

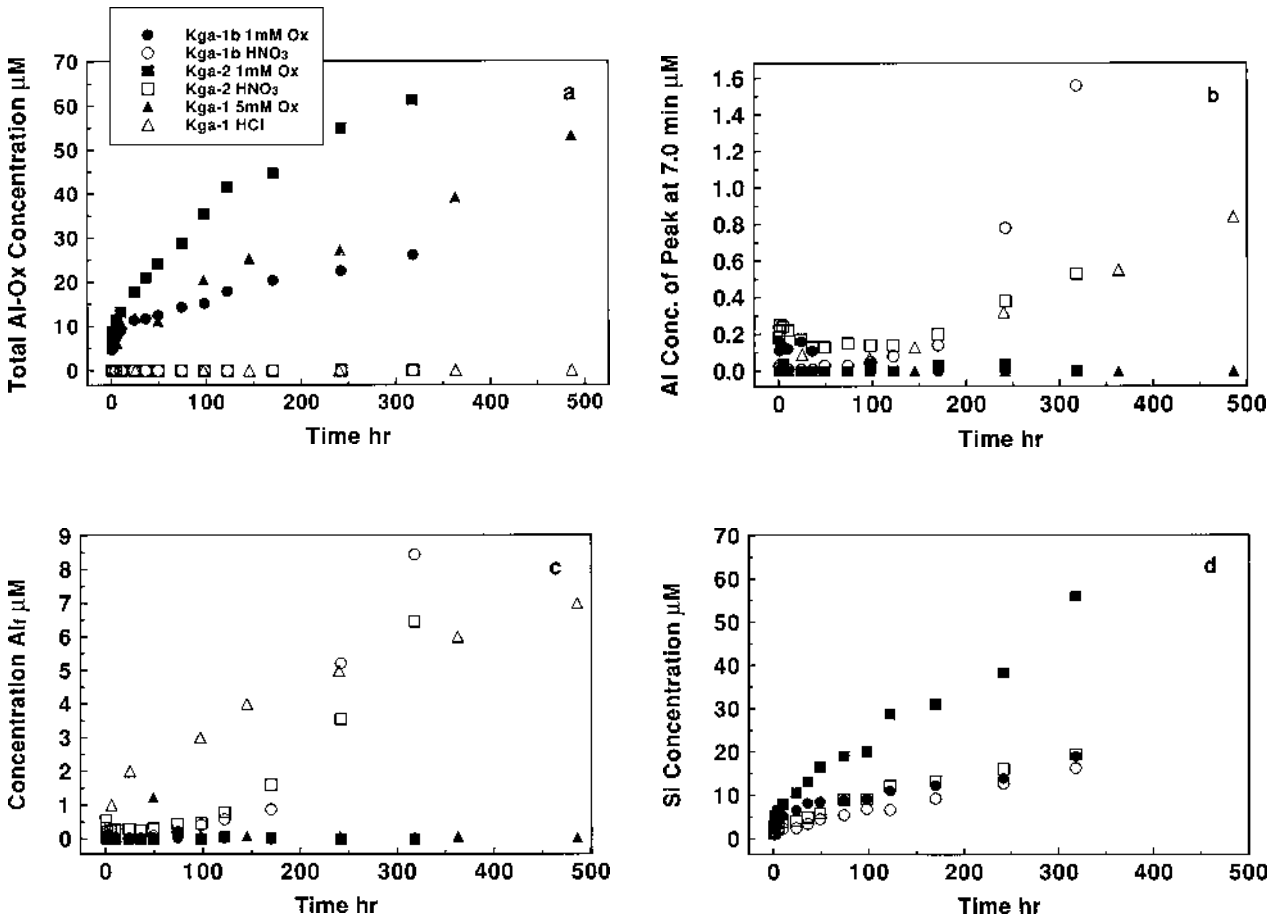

FIGURE 3. (a, b, and c) Al species distributions over the course of KGa-1b and KGa-2 dissolution in organic and inorganic acids, as measured by HP-CEC. **(a)** Al-Oxalate **(b)** peak at ~7 min **(c)** Al_f, **(d)** Si. The legend shown in a is the same for all parts of Figures 3 and 4.

hydrothermal Cornwall kaolinite apparently dissolves slightly faster in oxalate solution than do the sedimentary kaolinites used in our study.

Nonlinear dissolution rates. The release data of dissolved monomeric Al in organic solutions and HCl and of Si in both inorganic and organic solutions (Figs. 3 and 4) show initial parabolic portions agreeing with other batch dissolution results for aluminosilicates with and without organic complexing ligands (Wollast 1967; Petrovic 1976; Holdren and Berner 1979; Berner 1981; Chin and Mills 1991). Such parabolic curves have variously been explained in terms of an experimental artifact caused by the presence of highly reactive fine particles or inhomogeneity of surface sites (Berner 1981; Chin and Mills 1991; Stillings et al. 1995). The ratio between R_{mAl} and oxalate sorption density (measured using initial minus reacted dissolved organic carbon concentration; data not shown here) was observed to decrease over the first 24 h of the dissolution experiment for KGa-1b and then to remain approximately constant. This suggests a change in dissolution mechanism within the first few hours of the experiment, perhaps due to removal of small reactive particles or amorphous material.

The rates of appearance of monomeric Al during the proton promoted dissolution of both kaolinites in pH 3.0 HNO_3 are highly nonlinear (Fig. 4c) with rates increasing over time. One hypothesis for this behavior may be that initial Al is released in forms (polymeric) that are not detected by our method, but this Al is later converted to measurable forms. As mentioned above, we did not anticipate the presence of stable polymeric Al in our experiments; indeed, initial Al^{3+} concentrations indicate that the system is highly undersaturated (five orders of magnitude or more in terms of Al^{3+} concentrations) with respect to the $Al_2(OH)_2^{4+}$ dimer. Unfortunately, we could not use total Al analysis to check for potential polymeric Al (by difference) because we measured Al concentrations at or below the operational detection limit of our graphite furnace AA (Clesceri et al. 1989). This is reasonable considering that our HP-CEC measurements of total monomeric Al concentrations during initial dissolution were on the order of 0.04 to 0.1 μM. Perhaps a better explanation for the curve shape may be Al readsorption during initial dissolution. Such readsorption has been suggested by both Wieland and Stumm (1992) and Schroth and Sposito (1997). If Al readsorption is occurring in our study systems, then it is occurring well below the so-called gibbsite solubility window (Sposito 1989) in samples greatly undersaturated with respect to gibbsite.

Congruency of dissolution. The dissolution of both kaolin-

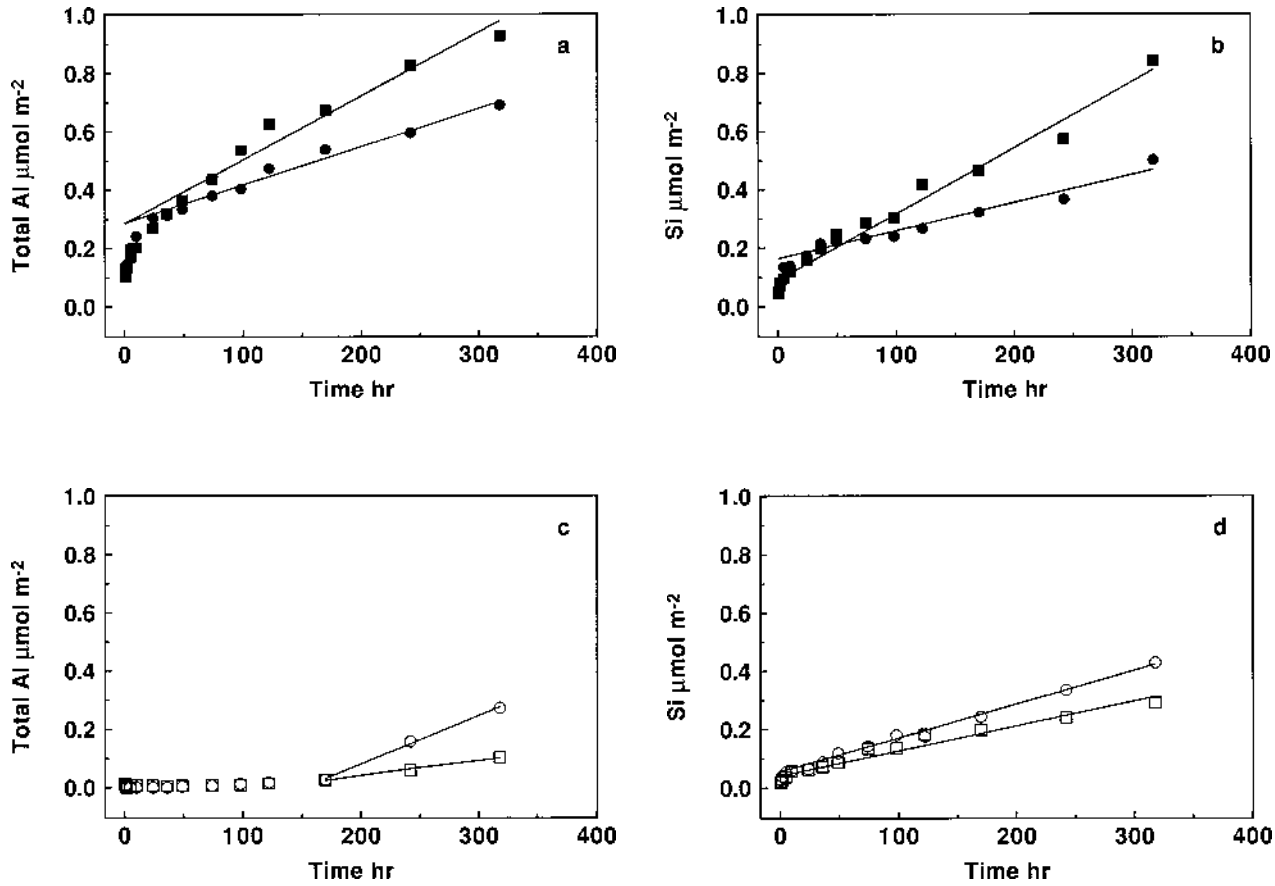

FIGURE 4. Al and Si release data for dissolution of KGa-1b and KGa-2 in organic and inorganic acids at pH 3, 22 °C. **(a)** Al release in 1 m*M* Oxalate **(b)** Si release in 1 m*M* Oxalate **(c)** Al release in HNO_3 **(d)** Si release in HNO_3. Solid lines indicate the points used in rate calculations.

ites in 1 m*M* oxalate appears to be nearly congruent, although R_{mAl} is somewhat higher than R_{Si} (based on data after 24 hours; Table 2). This is in agreement with Wieland and Stumm's (1992) observation of congruent dissolution of Cornwall kaolinite in oxalate at pH $\leq$4. It is difficult to determine congruency for our inorganic experiments, because we were unable to identify steady state. The concentration of Si released to solution is consistently higher than Al, although there is a tendency toward potential convergence over time. Wieland and Stumm (1992) reported $R_{Si} > R_{Al}$ for Cornwall kaolinite in HNO_3 at acidic pH values.

Use of 5 m*M* oxalate appears to increase the amount of monomeric Al released from KGa-1b approximately 8.5 times over the amount released in inorganic acid alone at 480 h reaction time. Rates cannot be compared for the inorganic curves for Al. For both KGa-1b and KGa-2, 1 m*M* oxalate in HNO_3 increased the amount of monomeric Al released relative to HNO_3 alone (Figs. 3 and 4). Si release was similar for inorganic vs. organic acids for KGa-1b. However, Si release was substantially greater in organic than inorganic solution for KGa-2. Both Chin and Mills (1991) and Wieland and Stumm (1992) reported a several-fold increase in Si release rates from kaolinite in the presence of oxalate.

Comparison of dissolution kinetics of kaolinites KGa-1b and KGa-2

For dissolution in 1 m*M* oxalate solution, R_{mAl} for KGa-2 (poorly crystallized) was approximately two times greater than R_{mAl} for KGa-1b (well crystallized). R_{Si} for KGa-2 was slightly more than two times greater than for KGa-1b. Many observed differences in surface and overall crystalline properties, micromorphology, microtopography, and specific surface area (Table 1) of the two kaolinites led to differences in dissolution rate in oxalate of only approximately a factor of 2 under our experimental conditions. KGa-2 has more irregular microtopography and is less crystalline; both of these factors may contribute to increased dissolution rates in the presence of oxalate. However, AFM measurements suggest that the ratio of edge to basal-plane surface areas are similar for the two samples (Table 1), and this may help to explain the similar dissolution rates. The comparability of rates for these two sedimentary kaolinites and the hydrothermal kaolinite studied by Wieland and Stumm (1992), suggests that it is the fundamental structure of kaolinite rather than specific surface details that exerted the greatest influence on dissolution kinetics.

The proton promoted dissolution rates of the two kaolinites, measured using Si, were similar with a slightly higher rate

for the well crystallized sample. Although R_{mAl} was not determined for the inorganic experiments, the amount of Al released at ~320 h was slightly higher for the well-crystallized sample than for the poorly crystallized sample. At first glance, it appears odd that the well crystallized sample dissolves slightly more rapidly than the poorly crystallized sample under inorganic conditions. One potential explanation may be that Al readsorption could be greater on the poorly crystallized sample, which has more complex microtopography, than to the well crystallized sample. At present, we cannot explain the very different dissolution behavior of KGa-1b in HCl than in HNO_3 at the same pH (Fig. 2c). The possibility that the presence of different anions Cl^- and NO_3^- may affect dissolution of kaolinite is presently under investigation.

ACKNOWLEDGMENTS

We thank the Petroleum Research Fund of the American Chemical Society for funding this research (grant to P.A.M.). We thank S. Cabaniss (Department of Chemistry, Kent State University) for helpful discussion regarding Al speciation, M. Jaroniec (Department of Chemistry, Kent State University) for BET measurements, and D. Eberl (U.S. Geological Survey, Boulder, Colorado) for discussion of XRD analyses and kaolinite structure. We thank B. Schroth and G. Sposito (University of California, Berkeley) for discussion of kaolinite cleaning methods. We thank K. Nagy, A. Blum, and E. Wieland for thoughtful reviews of the manuscript.

REFERENCES CITED

Bereznitski, Y., Jaroniec, M., and Maurice, P. (1998) Absorption characterization of two Clay Minerals Society standard kaolinites. Journal of Colloid and Interface Science, 205, 528–530.

Berner, R.A. (1981) Kinetics of weathering and diagenesis. In Mineralogical Society of America, Reviews in Mineralogy, 8, 69–110.

Berner, R.A. and Morse, J.W. (1974) Dissolution kinetics of calcium carbonate in sea water: IV. Theory of calcite dissolution. American Journal of Science, 274, 108–134.

Blum, A.E. (1994) Determination of illite/smectite particle morphology using scanning force microscopy. In K.L. Nagy and A.E. Blum, Eds., Scanning Probe Microscopy of Clay Minerals, 172–202. Clay Minerals Society, Boulder.

Brady, P.V., Cygan, R.T., and Nagy, K.L. (1996) Molecular controls on kaolinite surface charge. Journal of Colloid and Interface Science, 183, 356–364.

Brantley, S.L. and Chen, Y. (1995) Chemical weathering rates of pyroxenes and amphiboles. In Mineralogical Society of America Reviews in Mineralogy, 31, 119–172.

Cabaniss, S.E. (1987) TITRATOR: An interactive program for aquatic equilibrium calculations. Environmental Science and Technology, 21, 209–210.

Carroll, S.A. and Walther, J.V. (1990) Kaolinite dissolution at 25, 60, and 80 ˚C. American Journal of Science, 290, 797–810.

Chin, P.F. and Mills, G.L. (1991) Kinetics and mechanisms of kaolinite dissolution: effects of organic ligands. Chemical Geology, 90, 307–317.

Chou, L. and Wollast, R. (1985) Steady-state kinetics and dissolution mechanisms of albite. American Journal of Science, 285, 963–993.

Clesceri, L.S., Greeenberg, A.E., and Trussell, R.R. (Eds.) (1989) Standard Methods for the Examination of Water and Wastewater. American Public Health Association, Washington, D.C., Section 3113.

Dove, P.M. and Hochella, M.F. Jr. (1993) Calcite precipitation mechanisms and inhibition by orthophosphate: in situ observations by scanning force microscopy. Geochimica et Cosmochimica Acta, 57, 705–714.

Drever, J.I. (1988) The Geochemistry of Natural Waters, 437 p. Prentice Hall, Englewood Cliffs, New Jersey.

Ganor, J., Mogollon, J.L., and Lasaga, A.C. (1995) The effect of pH on kaolinite dissolution rates and on activation energy. Geochimica et Cosmochimica Acta, 59, 1037–1052.

Hochella, M.F. Jr. (1990) Atomic structure, microtopography, composition, and reactivity of mineral surfaces. In Mineralogical Society of America Reviews in Mineralogy, 23, 87–132.

Holdren, G.R. Jr. and Berner, R.A. (1979) Mechanism of feldspar weathering: I. Experimental studies. Geochimica et Cosmochimica Acta, 43, 1161–1171.

Martell, A.E., Smith, R.M., and Motekaitis (1993) NIST Critical Stability Constants of Metal Complexes Data Base (Computerized). NIST, Department of Commerce, Gaithersburg, Maryland, U.S.A.

Maurice, P.A. (1996) Application of atomic-force microscopy in environmental colloid and surface chemistry. Colloids and Surfaces A, 107, 57–75.

Maurice, P.A. and Lower, S.L. (1997) Use of atomic force microscopy in studying soil mineral reactions. Advances in Agronomy, 62, 1–43.

Nagy, K.L., Blum A.E., and Lasaga, A.C. (1991) Dissolution and precipitation kinetics of kaolinite at 80 °C and pH 3: The dependence on solution saturation state. American Journal of Science, 291, 649–686.

Petrovic, R. (1976) Rate control in feldspar dissolution II: the protective effect of precipitation. Geochimica et Cosmochimica Acta, 40, 1509–1522.

Prater, C.B., Maivald, P.G., Kjoller, K.J., and Heaton, M.G. (1995) Tapping mode imaging application and technology. Digital Instruments Nanonotes, Santa Barbara, California, U.S.A.

Rimstidt, J.D. and Dove, P.M. (1986) Mineral/solution reaction rates in a mixed flow reactor: wollastonite hydrolysis. Geochimica et Cosmochimica Acta, 50, 2509–2516.

Schroth, B. and Sposito, G. (1997) Surface charge properties of kaolinite. Clays and Clay Minerals, 45, 85–91.

Sposito, G. (1989) The Chemistry of Soils, 277 p. Oxford University Press, London.

Stillings, L.L., Brantley, S.L., and Machesky, M.L. (1995) Proton adsorption at an adularia feldspar surface. Geochimica et Cosmochimica Acta, 59, 1473–1482.

Sutheimer, S.H. and Cabaniss, S.E. (1995a) Determination of trace aluminum in natural waters by flow-injection analysis with fluorescent detection of the lumogallion complex. Analytica Chimica Acta, 303, 211–221.

——(1995b) Aqueous Al(III) speciation by high-performance cation exchange chromatography with fluorescence detection of the aluminum-lumogallion complex. Analytical Chemistry, 67, 2342–2349.

——(1997) Aluminum binding to humic substances determined by high-performance cation exchange chromatography. Geochimica et Cosmochimica Acta, 61, 1–9.

Van Olphen, H. and Fripiat, J.J. (Ed.) (1979) Data Handbook for Clay Minerals and Other Non-Metallic Minerals. Pergamon.

Wieland, E. and Stumm, W. (1992) Dissolution kinetics of kaolinite in acidic aqueous solution at 25 °C. Geochimica et Cosmochimica Acta, 56, 3339–3355.

Wollast, R. (1967) Kinetics of the alteration of K-feldspar in buffered solution at low temperature. Geochimica et Cosmochimica Acta, 31, 635–648.

Xie, Z. and Walther J. (1992) Incongruent dissolution and surface area of kaolinite. Geochimica et Cosmochimica Acta, 56, 3357–3363.

Zbik, M. and Smart, R.S. (1998) Nanomorphology of kaolinites: comparative SEM and AFM studies. American Mineralogist, 46, 2, 153–160.

Zhou, Q. (1996) Surface characteristics and dissolution kinetics of two standard kaolinites, Master's thesis, Kent State University, Kent, Ohio, U.S.A.

MANUSCRIPT RECEIVED MAY 1, 1998
MANUSCRIPT ACCEPTED OCTOBER 29, 1998
PAPER HANDLED BY KATHRYN L. NAGY